

Layer-resolved resonance intensity of evanescent polariton modes in anisotropic multilayersNikolai Christian Passler,¹ Xiang Ni,² Giulia Carini,¹ Dmitry N. Chigrin ,^{3,4} Andrea Alù,^{5,6} and Alexander Paarmann ^{1,*}¹*Fritz-Haber-Institut der Max-Planck-Gesellschaft, Faradayweg 4-6, 14195 Berlin, Germany*²*School of Physics, Central South University, Changsha, Hunan 410086, China*³*DWI-Leibniz-Institut für Interaktive Materialien, Forckenbeckstrasse 50, 52074 Aachen, Germany*⁴*Institute of Physics (IA), RWTH Aachen University, 52074 Aachen, Germany*⁵*Photonics Initiative, Advanced Science Research Center, City University of New York, New York, New York 10031, USA*⁶*Physics Program, Graduate Center, City University of New York, New York, New York 10016, USA*

(Received 5 September 2022; revised 26 April 2023; accepted 24 May 2023; published 27 June 2023)

Phonon polariton modes in layered anisotropic heterostructures are a key building block for modern nanophotonic technologies. The light-matter interaction for evanescent excitation of such a multilayer system can be theoretically described by a transfer-matrix formalism. This method allows us to compute the imaginary part of the p -polarized reflection coefficient $\text{Im}(r_{pp})$, whose resonant features are commonly used to evaluate the polariton dispersion of the multilayer structure. This reflection coefficient, however, does not reveal how the different layers contribute to these resonances. We present an approach to compute layer-resolved polariton resonance intensity in arbitrarily anisotropic layered heterostructures, based on calculating the Poynting vector extracted from the transfer-matrix formalism under evanescent light excitation. Our approach is independent of the experimental excitation conditions, and it fulfills a strictly proved conservation law for the energy flux. As a testing ground, we study two state-of-the-art nanophotonic multilayer systems, covering strong coupling and tunable hyperbolic surface phonon polaritons in twisted MoO_3 double layers. Providing a new level of insight into the polaritonic response, our method holds great potential for understanding, optimizing, and predicting new forms of polariton heterostructures in the future.

DOI: [10.1103/PhysRevB.107.235426](https://doi.org/10.1103/PhysRevB.107.235426)**I. INTRODUCTION**

Layered heterostructures provide a versatile platform for the construction of nanophotonic devices, enabling extensive functionality of light propagating through nanoscale stratified systems [1]. The tremendous progress reported using layered systems is significantly fueled by polaritons—strong light-matter interaction featuring strongly localized, immense electric field strengths—advancing a variety of nanophotonic fields such as optoelectronics [2,3], photovoltaics [4,5], polaritonic optics [6–8], or sensing [9]. In particular, layered systems that are composed of strongly optically anisotropic polar crystals currently receive increasing interest due to their capability of supporting infrared polariton modes of high propagation directionality, so called hyperbolic phonon polaritons (hPhP) [10–14]. While in isotropic polar crystals, phonon polaritons arise in the frequency region of negative permittivity between the transverse optical (TO) and longitudinal optical (LO) phonon modes, hPhPs in anisotropic

crystals arise at frequencies where the permittivity is only negative along one (type I hyperbolic) or two (type II hyperbolic) principal crystal axes. Thin films of materials with out-of-plane anisotropy, such as hexagonal boron nitride (hBN), support volume-confined hPhPs, which have proven to enable subdiffraction imaging and hyperlensing [15,16]. Materials with strong in-plane anisotropy, such as molybdenum trioxide (MoO_3), on the other hand, support in-plane hyperbolic phonon polaritons (ihPhPs) featuring directional propagation in the surface plane. The potential of these materials has only recently captured attention, as demonstrated in particular by the seminal work of several groups on twisted MoO_3 layers [17–21], where the twist angle enables control over the ih-PhP wavefront geometries, propagation characteristics, and its topology.

Advances in the field of polaritonic nanophotonics often are only feasible with the aid of a robust theoretical framework for the simulation of the optical response of the material system in question. For layered heterostructures, a 4×4 transfer-matrix method (TMM) [22] has proven useful in this context, as it is able to provide the reflection and transmission coefficients as well as the local electric fields of a multilayer system consisting of any number of arbitrarily anisotropic materials. Furthermore, the analysis of the Poynting vector \mathcal{S} allows for a layer-resolved calculation of the absorption and transmittance in the system even for fully anisotropic constituent materials [23]. However, strongly confined polaritons typically are evanescent modes, i.e., they feature in-plane

*alexander.paarmann@fhi-berlin.mpg.de

momenta k larger than the momentum of light in vacuum k_0 , and thus they cannot be accessed in a free-space excitation scheme. This condition for the excitation has to be accounted for in both the experimental as well as the theoretical observation of polaritons, and it is met, for instance, in prism-coupling techniques such as the Otto geometry [24–26] or the Kretschmann-Raether configuration [27]. While in particular the Otto geometry allows for a systematic, thorough study of phonon polaritons and has proven to be quite versatile [8,28–30], the intrinsic properties of the polariton modes in the sample are inevitably modified by the presence of the coupling prism. Other optical excitation techniques where large momenta are achieved by scattering off a nanoscale object, such as scattering-type scanning near-field optical microscopy (s-SNOM) [31,32], on the other hand, cannot fully be described theoretically using a 4×4 transfer-matrix method, due to the deviation from a stratified system by the scattering source.

A common way to circumvent the specifics of the excitation method in the simulations is to calculate the optical response solely of the sample, with an excitation beam featuring large in-plane momenta $k/k_0 > 1$. This evanescent wave excitation has proven insightful into the supported polariton mode dispersion [6,29,33–36]. In particular, the imaginary part of the p -polarized reflection coefficient $\text{Im}(r_{pp})$ is known to peak at frequencies where the system supports a polariton mode, thus providing a means to map out the intrinsic polariton dispersion. Here, the reflection coefficient r_{pp} is the ratio of the p -polarized component of the reflected field and the p -polarized incident field. It is well established that any guided mode of a system is linked to poles in the scattering coefficients [37]. In layered heterostructures comprising several materials that support polaritons, however, the method of using $\text{Im}(r_{pp})$ only reveals the resonances of the overall system, while it remains unresolved how the different layers contribute to that resonance. For plane-wave far-field excitations with $k/k_0 < 1$, a layer-resolved calculation framework for energy flux and absorption in anisotropic multilayers has been explored [23], but to the best of our knowledge an equivalent method for evanescent excitation with $k/k_0 > 1$ has not been discussed in the literature so far.

Here, we present an approach for layer-resolved calculation of the relative intensity of polariton resonances in arbitrarily anisotropic layered heterostructures by analyzing the light absorption under evanescent excitation. The method of using $\text{Im}(r_{pp})$ for the determination of the polariton dispersion has been successfully and continuously used for several years. The peak positions coincide with resonant modes of the system, in particular in the absence of loss, where the poles of the reflection coefficient reveal the system's guided modes [37]. For real systems with finite loss, however, the amplitude of these resonances is usually not discussed, and analysis of these amplitudes has remained empirical. Here we build on this empirical knowledge, expanding the established method of analyzing $\text{Im}(r_{pp})$ by a layer-resolved calculation of energy flow based on the Poynting vector obtained from a 4×4 TMM. In particular, we introduce and strictly prove a conservation law for the energy flow in the system that is valid for evanescent excitations. Our method is then implemented in an open-access computer program [38]. We demonstrate

the power of our method by calculating the layer-resolved polariton resonances in two state-of-the-art polaritonic systems, covering strongly coupled surface phonon polaritons (SPhPs) in an aluminum nitride (AlN)/silicon carbide (SiC) heterostructure, and tunable ihPhPs in twisted MoO₃ layers on a quartz (SiO₂) substrate. The relative intensity of the polariton resonances in the different layers of the sample systems provides new insight into the formation mechanisms of polaritons in complex heterostructures, and will thus prove very useful in guiding the targeted design of polariton structures.

II. METHOD

The TMM we employ in this work has been described in detail previously [22]. For the calculation of the layer-resolved polaritonic response of the sample system, we further use an extended formalism based on the TMM [23], providing the time-averaged Poynting vector $\vec{S}_i^p(z)$ for p -polarized incident light, in layer i , at position z :

$$\vec{S}_i^p(z) = \frac{1}{2} \text{Re}[\vec{\mathcal{E}}_i^p(z) \times \vec{\mathcal{H}}_i^{p*}(z)], \quad (1)$$

where $\vec{\mathcal{E}}_i(z)$ and $\vec{\mathcal{H}}_i(z)$ are given elsewhere [23]. Note that this formalism is originally designed for propagating incident light with $k/k_0 < 1$. Further on [Eq. (5)], we extend the method to evanescent excitation with $k/k_0 > 1$. The coordinate system is chosen such that the z -axis points along the surface normal, the exciting light beam is incident in the $x - z$ -plane, and the origin of the coordinate system lies in the interface plane between the isotropic, lossless semi-infinite incident medium ($i = 0$) and the first layer ($i = 1$). The multilayer system comprises N layers of thicknesses d_i , and layer $i = N + 1$ is the semi-infinite substrate. Because polaritons are typically excitable by p -polarized light [8], we focus on p -polarization in the following and omit the specification of the incoming polarization.

To calculate the transmittance up to layer i and position z , the z -component of the Poynting vector at the corresponding position is normalized by the z -component of the Poynting vector of the incoming excitation beam $\mathcal{S}_{\text{inc},z}$:

$$\mathcal{T}_i(z) = \frac{\mathcal{S}_i^z(z)}{\mathcal{S}_{\text{inc}}^z}, \quad (2)$$

and the transmittance \mathcal{T} into the substrate $i = N + 1$ at the interface with layer N is given by

$$\mathcal{T} = \frac{\mathcal{S}_{N+1}^z(D)}{\mathcal{S}_{\text{inc}}^z}, \quad (3)$$

where $D = \sum_{i=1}^N d_i$ is the thickness of the multilayer system. Using Eq. (2), the layer-resolved absorption can be calculated as follows:

$$\mathcal{A}_i = \mathcal{T}_i(d_{1,\dots,i-1}) - \mathcal{T}_i(d_{1,\dots,i-1} + d_i), \quad (4)$$

where $d_{1,\dots,i-1} = \sum_{i=1}^{i-1} d_i$ is the thickness of all layers through which the incident light has propagated before reaching the layer i .

For a propagating excitation beam with $k/k_0 < \epsilon_0$, $\mathcal{S}_{\text{inc}}^z$ is real-valued, as specified in Eq. (22) of Ref. [23], and \mathcal{A} and

\mathcal{T} correctly describe the absorption and transmission, respectively. For an evanescent incident beam with $k/k_0 > 1$ in the isotropic, lossless incident medium, however, $\mathcal{S}_{\text{inc}}^z$ is purely imaginary, since an evanescent beam features no net energy flow in the z -direction. As a consequence, for evanescent excitation, this would lead to a zero denominator in Eq. (2). Here, we therefore normalize to the imaginary part of $\mathcal{S}_{\text{inc}}^z$ instead, as can be calculated from Eq. 22 of Ref. [23] with the following modification:

$$\vec{\mathcal{S}}_{\text{inc}}(0) = \frac{1}{2} \text{Im}[\vec{\mathcal{E}}_{0,\text{inc}}(0) \times (\vec{k}_{0,\text{inc}} \times \vec{\mathcal{E}}_{0,\text{inc}}(0))^*], \quad (5)$$

where $\vec{\mathcal{E}}_{0,\text{inc}}(0)$ is the electric field of the incoming evanescent wave at the first interface at $z = 0$, and $\vec{k}_{0,\text{inc}}$ is the wave vector of the p -polarized incident beam.

The layer-resolved ‘‘absorption’’ calculated according to Eq. (4) conveniently reflects the relative intensities of a polariton mode present in the different layers of a multilayer structure, as we will demonstrate in the following section. Analogously to $\text{Im}(r_{pp})$, \mathcal{T} and \mathcal{A} take values larger than 1 in the case of $k/k_0 > \varepsilon_0$, as expected in the case of evanescent excitations.

Strikingly, the sum of the layer-resolved quantities \mathcal{A}_i and \mathcal{T} fulfills the following conservation law:

$$2 \text{Im}(r_{pp}) = \sum_{i=1}^N \mathcal{A}_i + \mathcal{T}, \quad (6)$$

where we calculate r_{pp} employing a TMM [22]. This equation constitutes the conservation between the resonance intensity distributed between the layers of the system described by \mathcal{A}_i and \mathcal{T} , and the overall resonance intensity, here found to be $2 \text{Im}(r_{pp})$.

Proof of the conservation law

In the following, we will strictly prove Eq. (6) for arbitrarily anisotropic heterostructures provided that the medium from which the wave impinges is refractive, lossless, and isotropic [$\text{Re}(\varepsilon_0) > 0$ and $\text{Im}(\varepsilon_0) = 0$]. Let us us specifically consider the first interface of such a heterostructure, between the incident medium and the first layer with arbitrarily anisotropic permittivity ε_1 . The incident p -polarized light will be evanescent for $q_x^2 > \varepsilon_0$, where q_x is the normalized in-plane momentum $q_x = k_x/k_0$ conserved throughout the heterostructure. Without loss of generality, we can write the incident and reflected electric fields at $z = 0$ as $\vec{\mathcal{E}}_{\text{inc}} = (q_{zi}, 0, q_x)$ and $\vec{\mathcal{E}}_{\text{refl}} = r_{pp}(-q_{zi}, 0, q_x) + r_{ps}(0, q_x, 0)$, and the corresponding magnetic fields as $\vec{\mathcal{H}}_{(\text{inc})} = (0, \varepsilon_0, 0)$ and $\vec{\mathcal{H}}_{\text{refl}} = r_{pp}(0, \varepsilon_0, 0) + r_{ps}(q_{zi}q_x, 0, -q_x^2)$, where $q_{zi} = \sqrt{\varepsilon_0 - q_x^2}$ is the normal-to-surface component of the incident momentum, and r_{pp} and r_{ps} are the p -pol-in p -pol-out and p -pol-in s -pol-out reflection coefficients, respectively.

Invoking the continuity of the incident, reflected, and transmitted in-plane fields $\mathcal{E}_1^x = \mathcal{E}_{0,\text{inc}}^x + \mathcal{E}_{0,\text{refl}}^x$ and $\mathcal{H}_1^y = \mathcal{H}_{0,\text{inc}}^y + \mathcal{H}_{0,\text{refl}}^y$ at the interface allows for explicit expressions for the transmitted Poynting vector at $z = 0$ right behind the interface

in medium 1:

$$\begin{aligned} \text{Re}(\mathcal{S}_1^z)(z=0) &= \text{Re}(\vec{\mathcal{E}}_1 \times \vec{\mathcal{H}}_1^*)^x \\ &= \text{Re}(\vec{\mathcal{E}}_{0,\text{inc}} \times \vec{\mathcal{H}}_{0,\text{inc}}^* + \vec{\mathcal{E}}_{0,\text{refl}} \times \vec{\mathcal{H}}_{0,\text{refl}}^* \\ &\quad + \vec{\mathcal{E}}_{0,\text{inc}} \times \vec{\mathcal{H}}_{0,\text{refl}}^* + \vec{\mathcal{E}}_{0,\text{refl}} \times \vec{\mathcal{H}}_{0,\text{inc}}^*)^z \\ &= \text{Re}(\varepsilon_0 q_{zi}(r_{pp}^* - r_{pp})) \\ &= 2\varepsilon_0 \sqrt{q_x^2 - \varepsilon_0} \text{Im}(r_{pp}), \end{aligned} \quad (7)$$

where we made use of $\text{Re}(\vec{\mathcal{E}}_{0,\text{inc}} \times \vec{\mathcal{H}}_{0,\text{inc}}^*)^z = \text{Re}(\vec{\mathcal{E}}_{0,\text{refl}} \times \vec{\mathcal{H}}_{0,\text{refl}}^*)^z = 0$, as well as $\text{Re}(-iq_{zi}) = \sqrt{q_x^2 - \varepsilon_0}$. Please note that the reflected cross-polarized electric (magnetic) field components that arise for birefringent media do not contribute to the energy flow since they are inherently parallel to the respective incident magnetic (electric) field, respectively, such that the cross products vanish. For a non-birefringent medium where ε_1 is a diagonal tensor, r_{ps} vanishes and Eq. (7) also holds. Finally, since $\text{Im}(\mathcal{S}_{0,\text{inc}}^z) = \text{Im}(\mathcal{E}_{0,\text{inc}} \times \mathcal{H}_{0,\text{inc}}^*)^z = \text{Im}(q_{zi}\varepsilon_0) = \varepsilon_0 \sqrt{q_x^2 - \varepsilon_0}$, we find that

$$\frac{\text{Re}(\mathcal{S}_1^z)}{\text{Im}(\mathcal{S}_{0,\text{inc}}^z)}(z=0) = \mathcal{T}(z=0) = 2 \text{Im}(r_{pp}). \quad (8)$$

Equation (8) strictly links the energy content of the light field at the first interface $\text{Re}(\mathcal{S}_1^z)(z=0)$ to $\text{Im}(r_{pp})$. Since $\text{Re}(\mathcal{S}_1^z)(z)$ describes the real energy flow, it needs to be strictly monotonous with increasing z , such that Eq. (8) together with Eqs. (2)–(4) directly proves Eq. (6) for any heterostructure, provided the incident medium is isotropic and lossless. Equivalent expressions can also be derived for s -polarized evanescent excitation.

This finding justifies quantitatively the common use of $\text{Im}(r_{pp})$ to determine the polariton resonances in the heterostructure. The resonance peaks correspond to enhancement of energy flow into the heterostructure. Thus, our results show that $\text{Im}(r_{pp})$, and in particular its amplitude, can be directly related to absorptive resonances not just qualitatively but also quantitatively, where also the contribution of energy flow into the substrate \mathcal{T} should be accounted for.

In the following, we will apply our method to two sample systems that have been discussed in recent literature, demonstrating that our results are not only in accordance with previous findings, but they also provide additional insights into the resonance behavior of polariton modes in layered heterostructures.

III. STRONGLY COUPLED ENZ POLARITONS

At frequencies close to zero crossings of the real part of the dielectric permittivity ε , a material features epsilon-near-zero (ENZ) light propagation with remarkable properties of the ENZ photonic modes [39], such as high emission directionality [40,41], enhanced nonlinear-optical conversion efficiency [42,43], and tunneling through narrow distorted waveguide channels [44,45]. In a polar crystal, ENZ conditions are met at the LO phonon frequency ω_{LO} , and an ENZ polariton can

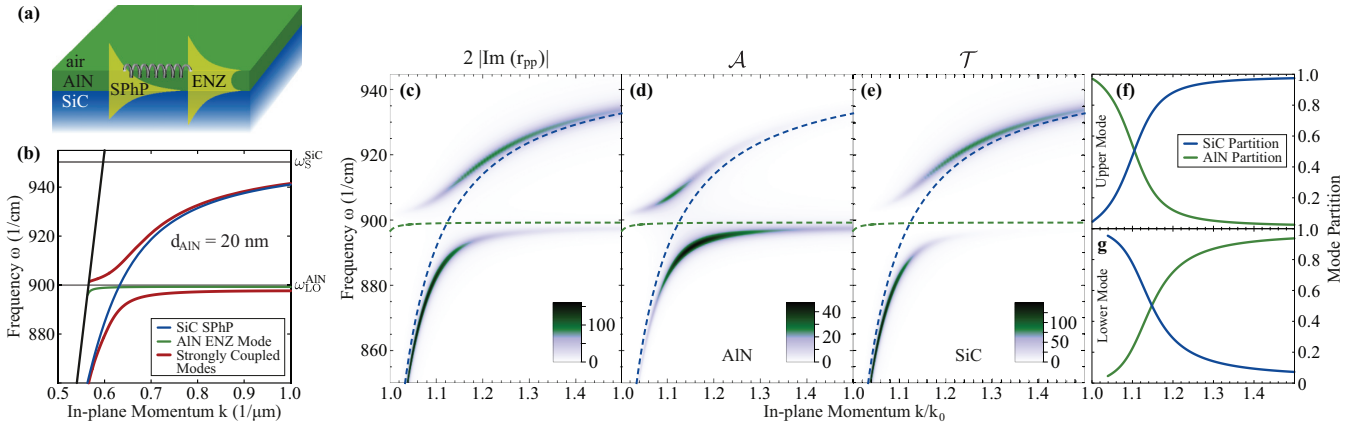


FIG. 1. Strong coupling between an AlN ENZ mode and a SiC SPhP. (a) Sketch of the AlN/SiC structure, illustrating the strong coupling of a SPhP of a bare SiC substrate and an ENZ mode of a freestanding AlN film. (b) Analytical dispersion of the uncoupled SiC SPhP (blue line) and AlN ENZ mode (green line), as well as the resulting strongly coupled modes in the heterostructure (red lines) featuring an avoided crossing. (c) Dispersion of the strongly coupled modes obtained by calculating the total resonance intensity $\text{Im}(r_{pp})$. (d), (e) Layer-resolved distribution of the resonance intensity in AlN and SiC, respectively. In (c), (d), and (e), the analytical dispersions of the uncoupled SiC SPhP (blue lines) and AlN ENZ modes (green lines) are plotted for reference. (f), (g) Mode partition of the AlN film and the SiC substrate for the upper and the lower dispersion branch, respectively.

be found in subwavelength-thin polar crystal films [46–48]. However, a thin-film ENZ polariton is a nonpropagating mode due to its intrinsically flat dispersion close to ω_{LO} , thus hindering its usability for effective nanoscale communication applications. This limitation can be overcome by strongly coupling an ENZ polariton to a propagating SPhP, as has been demonstrated for an aluminum nitride (AlN) thin film/silicon carbide (SiC) heterostructure [29]; see Fig. 1(a). By combining the advantages of the constituent uncoupled modes, the resulting ENZ-SPhPs feature strong electrical field enhancement characteristic for ENZ modes, while maintaining a propagative character typical for SPhPs.

The dispersions of both the uncoupled AlN ENZ mode (green line) and the SiC SPhP (blue line) as well as the strongly coupled modes (red lines) are plotted in Fig. 1(b), calculated with an analytical formula for a three-layer system [48,49]. Characteristically for strong coupling, the ENZ-SPhP dispersion lines exhibit an avoided crossing while approaching the dispersion lines of the uncoupled modes with increasing distance to the dispersion crossing point. Accordingly, the mode nature along each of the strongly coupled mode dispersions undergoes a transition across the avoided crossing, while at the avoided crossing, both strongly coupled modes have identical characteristics such as electric field enhancement and spatial confinement [29], sharing equal measures of both uncoupled modes. To verify and visualize this transition of mode nature across the strong-coupling region, we apply our method here to calculate the polariton resonance intensity in the AlN/SiC heterostructure resolved for each layer.

The overall polaritonic response of the material system can be obtained by calculating $\text{Im}(r_{pp})$, as is shown in Fig. 1(c), where the entire dispersions of both strongly coupled modes are reproduced. The layer-resolved calculations obtained from our method are plotted in Fig. 1(d) (\mathcal{A} in AlN) and Fig. 1(e) (\mathcal{T} in SiC). For both layers, only parts of the same dispersion

lines as for $\text{Im}(r_{pp})$ are obtained. In the AlN film [Fig. 1(d)], the resonance intensity is strongest in close proximity to the AlN ENZ mode (green line), whereas the intensity fades out along the SiC SPhP (blue line). In the SiC substrate [Fig. 1(e)], on the contrary, the resonance intensity is most pronounced along the SiC SPhP, and almost no intensity can be found along the AlN ENZ mode. This relative intensity distribution between the different layers reflects the respective partial mode nature along the dispersion, changing from the AlN ENZ mode to the SiC SPhP and vice versa. This behavior can be demonstrated by quantifying the mode partition \mathcal{P} as follows:

$$\mathcal{P}_i = \frac{\mathcal{A}_i}{2\text{Im}(r_{pp})}, \quad (9)$$

and evaluating \mathcal{P}_{SiC} and \mathcal{P}_{AlN} (blue and green lines) along both dispersion branches of the strongly coupled polariton modes, as shown in Figs. 1(f) and 1(g), respectively. Clearly, along both branches the mode nature undergoes the aforementioned transition, with a crossing point where the mode exhibits AlN ENZ and SiC SPhP features in equal measures. Notably, this crossing point sits at slightly different in-plane momenta for the upper and the lower branch, corresponding to the momentum where the uncoupled mode dispersions are equidistant to the respective branch in frequency-momentum space.

An alternative approach to obtain the relative mode distribution in the multilayer system would be to calculate the layer-resolved absorption for excitation with a propagating wave ($k/k_0 < 1$) via Otto-type prism coupling. However, in this scheme, the relative absorption of the polariton modes is distorted by the coupling prism, because the AlN ENZ and the SiC SPhP modes feature distinct critical gaps of optimal coupling conditions. In contrast, our approach is free of the influence of the excitation method, revealing consistent additional information about the mode nature of the strongly coupled modes in the AlN/SiC heterostructure.

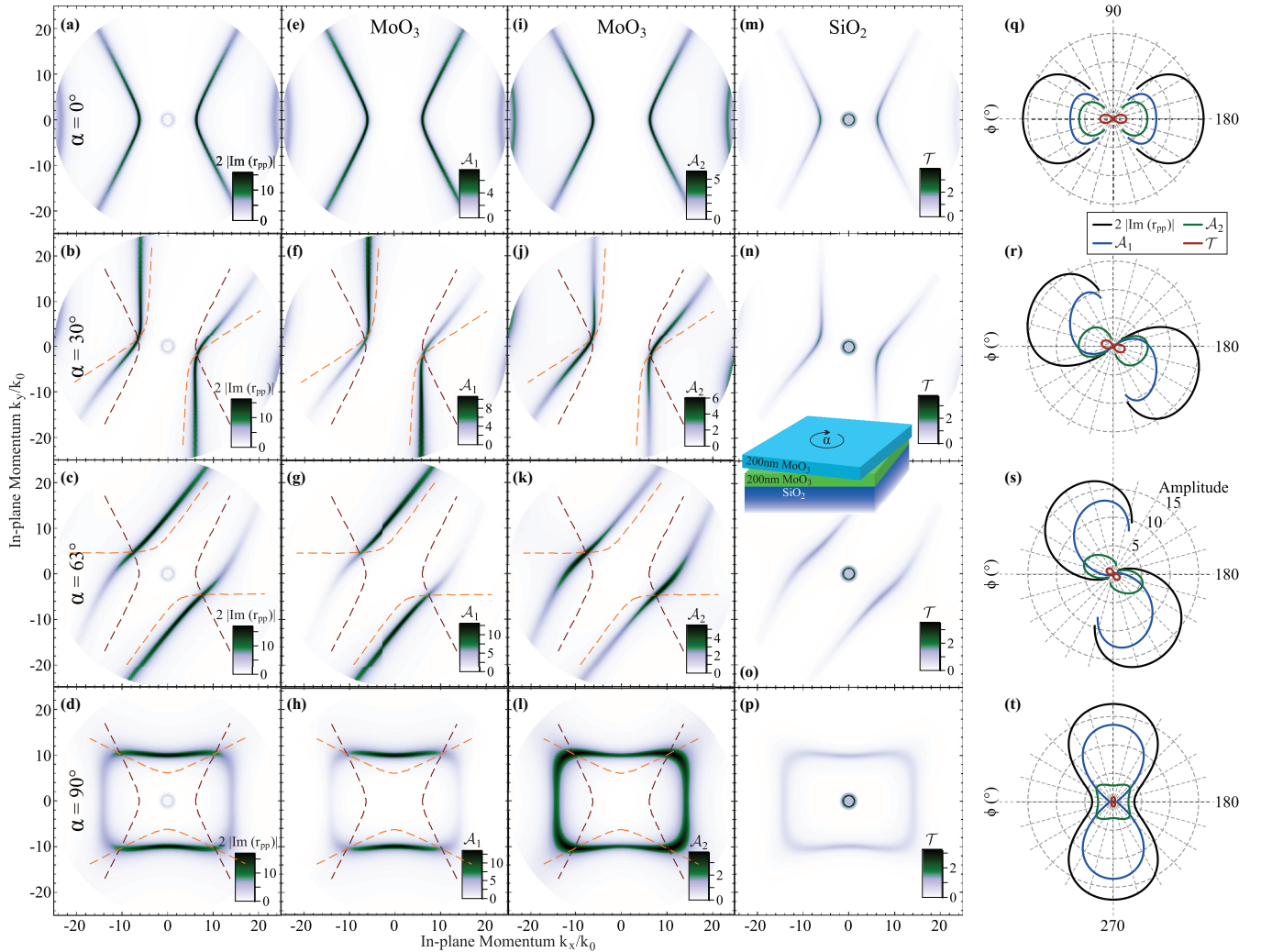


FIG. 2. Tunable phonon polaritons in twisted MoO₃ layers. (a)–(d) $\text{Im}(r_{pp})$ as a function of in-plane momenta k_x/k_0 and k_y/k_0 for a 200 nm MoO₃/200 nm MoO₃/SiO₂ heterostructure, as illustrated in the inset, at four different twist angles $\alpha = 0^\circ, 30^\circ, 63^\circ, 90^\circ$ of the upper MoO₃ layer, respectively. The calculations reveal a topological transition at the magic twist angle $\alpha^* = 63^\circ$ from an ihPhP to an elliptical SPhP. We also show the expected dispersion for each individual rotated MoO₃ layer as bright red (top layer) and dark red (bottom layer) dashed lines, to illustrate how the total dispersion relates to the dispersion of each layer. (e)–(h) Layer-resolved resonance intensity A_1 in the upper and (i)–(l) in the lower MoO₃ layer, (m)–(p) \mathcal{T} in the SiO₂ substrate, and (q)–(t) polar plots of the resonance intensities of all four quantities along the dispersion of the first-order SPhP mode, each at four different twist angles α , respectively.

IV. IN-PLANE HYPERBOLIC POLARITONS IN TWISTED MoO₃ LAYERS

In-plane hyperbolic phonon polaritons (ihPhPs) are supported on polar crystals with in-plane hyperbolicity, that is, at frequencies where $\text{Re}(\epsilon_x)\text{Re}(\epsilon_y) < 0$ (with the crystal surface lying in the $x - y$ -plane). The dispersion of ihPhPs takes the form of a hyperbola in the surface plane, oriented such that the hyperbola minimum lies on the crystal axis along which $\text{Re}(\epsilon) < 0$, whereas no solution is supported along the perpendicular surface direction where $\text{Re}(\epsilon) > 0$. Therefore, ihPhPs intrinsically feature a strong propagation directionality. At frequencies where both in-plane permittivity tensor elements are negative, on the other hand, the dispersion describes an ellipse, and the resulting SPhP can propagate along any direction in the surface plane.

Recently, it has been demonstrated that by stacking and twisting two MoO₃ layers, the propagation direction of the supported surface polaritons becomes configurable as a function of the twist angle α [17,18,20]. Furthermore, at a specific, frequency-dependent magic angle, the surface polariton performs a topological transition from a hyperbolic to an elliptical dispersion. The overall change in propagation direction and topology as a function of α is well-captured by $\text{Im}(r_{pp})$, as is reproduced in Figs. 2(a)–2(d) in perfect agreement with the literature. At twist angles $\alpha = 0^\circ$ and 30° [Figs. 2(a) and 2(b), respectively], the polariton is hyperbolic, and the propagation direction rotates with α . At the magic angle $\alpha^* = 63^\circ$, the dispersion transitions from hyperbolic to elliptical, resulting in flattened dispersion lines that exhibit diffractionless and low-loss directional polariton canalization [17]. Finally, at $\alpha = 90^\circ$ [Fig. 2(d)], the topological transition

is completed and the stacked system features an “elliptical” dispersion (that is, finite in all in-plane directions) of almost rectangular shape.

To reveal the optical response resolved for each material layer of the twisted heterostructure, we employ our formalism to calculate \mathcal{A}_1 and \mathcal{A}_2 for the two MoO₃ layers, and \mathcal{T} for the SiO₂ substrate [the system is sketched in the inset in Fig. 2(o)]. The resonance intensities \mathcal{A}_1 and \mathcal{A}_2 for the four twist angles $\alpha = 0^\circ, 30^\circ, 63^\circ, 90^\circ$ in the first and second MoO₃ layers are shown in Figs. 2(e)–2(h) and 2(i)–2(l), respectively, and the resonance intensity \mathcal{T} in the substrate is plotted in Figs. 2(m)–2(p). For $\alpha = 30^\circ, 63^\circ, 90^\circ$, we additionally plot the expected dispersion for each of the two layers (in bright and dark red dashed lines) without twist, as extracted from Fig. 2(a). There are at least two general observations of interest in these plots. (i) The twisted bilayer dispersion follows the single-layer dispersion in part (either the top layer or the bottom layer dispersion), but generally offset to larger momenta. This can be understood as a continuous transition from a single thick layer to two thinner layers each supporting higher momentum states. Still, the full dispersion always coincides with the crossing points of the single-layer dispersion. (ii) The resonance intensity in each layer is generally strongest when the bilayer dispersion is aligned with its individual dispersion, and suppressed otherwise.

Overall, we observe a stark imbalance of how both MoO₃ layers contribute to the response, which is dominated by the top layer. This asymmetry between both layers becomes clear when we analyze the resonance intensity peak value along the dispersion of the first-order mode shown in polar plots in Figs. 2(q)–2(t). Note that the curves are not continuous for $\alpha = 0^\circ, 30^\circ$, and 63° because of the finite plot range and the divergent nature of the hyperbolic dispersion. The maximum resonance intensity is strongest in the first MoO₃ layer and decreases towards the substrate [Figs. 2(q)–2(t)]. As a consequence, rotating the first layer dominates the overall maximum intensity along the dispersion in $\text{Im}(r_{pp})$ (black lines), which rotates with α . The same is true for \mathcal{T} in the isotropic SiO₂ substrate (red lines). The intensity maxima of \mathcal{A}_1 and \mathcal{A}_2 in the first and second MoO₃ layer, however, follow the orientation of the optical axis in the respective layer, where in the first layer (blue lines), the maximum is shifted clockwise in the direction of the twist rotation, while in the second layer (green lines), the maximum is only mildly rotated. This leads to strongly asymmetric intensity distributions along the dispersion in both MoO₃ layers for the hyperbolic region, that is, at twist angles $\alpha = 30^\circ$ and 63° [Figs. 2(f) and 2(j) and Figs. 2(g) and 2(k), respectively]. At $\alpha = 90^\circ$, finally, the intensity maximum is oriented along the y -axis and arises mostly from the first MoO₃ layer, while the small fraction of resonance intensity along the x -axis solely originates in the second layer.

By resolving the spatial origin of the resonance intensity layer by layer, our method reveals that the partial resonance intensity in each MoO₃ film is oriented along the respective polariton-active crystal axis. However, due to the presence of the respective other MoO₃ layer, the partial response in each MoO₃ film can feature strongly asymmetric azimuthal

intensity distributions, depending on the twist angle α . Thus, the polariton modes of the individual films are modified by the presence of the adjacent twisted MoO₃ film, while not featuring full hybridization, as has been observed in the previous example system. Thus, the resulting polariton mode in the full system cannot easily be seen as the sum of these partial polaritonic responses in each MoO₃ layer. Revealing this layer-resolved information, our method therefore provides a deeper analysis of the supported ihPhP modes for each topological state in the twisted MoO₃ double-layer heterostructure, and it may even accomplish the guiding principles for engineering the dispersion.

V. DISCUSSION

The presented method reveals unprecedented details on the polariton distribution in multilayer systems at low computational cost. Following the recent success of twisted double-layer structures, we anticipate a high demand for modeling forthcoming twisted multilayer concepts. Here, our approach could provide comprehensive data that may significantly help to identify the guiding principles for designated design goals. If additionally the relevant physics is driven by the polariton intensity in a specific layer or at a given interface of the structure, as expected, for example, for polariton-driven chemistry, the relevance of our layer-resolved analysis is enhanced even further. As a natural extension, it would be highly desirable to be able to quantitatively connect the results obtained here to experimentally accessible quantities, as, for instance, the scattering amplitude and phase in nano-FTIR or s-SNOM, which would enable much enhanced data analysis capabilities for multilayer structures.

VI. CONCLUSION

In this work, we have presented an approach for the layer-resolved analysis of the resonance intensity of polariton modes in arbitrarily anisotropic, birefringent, and absorbing multilayer media. Our method builds on evaluating resonances in the imaginary part of the reflection coefficient $\text{Im}(r_{pp})$ for evanescent wave excitation that has been successfully used for identifying polariton resonances in the literature for several years. The resulting layer-resolved resonance intensities that we calculate from the Poynting vectors obtained from a TMM [22,23] fulfill a strictly proved conservation law, showing that the resonance intensity expressed in $\text{Im}(r_{pp})$ can be partitioned into a sum of the resonance intensities in each system layer which are directly connected to the energy flux through the structure. Thereby, our analysis also quantitatively links the resonance amplitudes $\text{Im}(r_{pp})$ to energy flow into the heterostructure under evanescent wave excitation. The presented method is implemented in an open-access computer program [38].

As case studies, we applied our approach to the analysis of two recently studied nanophotonic systems featuring strong coupling between an ENZ and a propagating SPhP mode and the modulation of the propagation direction and the topology of ihPhPs in a twisted bilayer, revealing yet undiscovered details about the supported polariton modes. By

enabling one to analyze any multilayer system independent of the excitation scheme, our method holds great potential for understanding, optimizing, and predicting new forms of polariton heterostructures in the future.

ACKNOWLEDGMENTS

We thank M. Wolf, S. Wasserroth, and R. Ernstorfer (FHI Berlin) for a careful reading of the manuscript, and M. Wolf and the Max Planck Society for supporting this work.

- [1] F. Xia, H. Wang, D. Xiao, M. Dubey, and A. Ramasubramaniam, *Nat. Photonics* **8**, 899 (2014).
- [2] K. He, C. Poole, K. F. Mak, and J. Shan, *Nano Lett.* **13**, 2931 (2013).
- [3] J. S. Ross, P. Klement, A. M. Jones, N. J. Ghimire, J. Yan, D. G. Mandrus, T. Taniguchi, K. Watanabe, K. Kitamura, W. Yao, D. H. Cobden, and X. Xu, *Nat. Nanotechnol.* **9**, 268 (2014).
- [4] E. Fortin and W. Sears, *J. Phys. Chem. Solids* **43**, 881 (1982).
- [5] W. J. Yu, Y. Liu, H. Zhou, A. Yin, Z. Li, Y. Huang, and X. Duan, *Nat. Nanotechnol.* **8**, 952 (2013).
- [6] T. G. Folland, A. Fali, S. T. White, J. R. Matson, S. Liu, N. A. Aghamiri, J. H. Edgar, R. F. Haglund, Y. Abate, and J. D. Caldwell, *Nat. Commun.* **9**, 4371 (2018).
- [7] K. Chaudhary, M. Tamagnone, X. Yin, C. M. Spägle, S. L. Oscurato, J. Li, C. Persch, R. Li, N. A. Rubin, L. A. Jauregui, K. Watanabe, T. Taniguchi, P. Kim, M. Wuttig, J. H. Edgar, A. Ambrosio, and F. Capasso, *Nat. Commun.* **10**, 4487 (2019).
- [8] N. C. Passler, A. Heßler, M. Wuttig, T. Taubner, and A. Paarmann, *Adv. Opt. Mater.* **8**, 1901056 (2020).
- [9] D. Rodrigo, O. Limaj, D. Janner, D. Etezadi, F. J. Garcia de Abajo, V. Pruneri, and H. Altug, *Science* **349**, 165 (2015).
- [10] Z. Jacob, *Nat. Mater.* **13**, 1081 (2014).
- [11] P. Li, M. Lewin, A. V. Kretinin, J. D. Caldwell, K. S. Novoselov, T. Taniguchi, K. Watanabe, F. Gaussmann, and T. Taubner, *Nat. Commun.* **6**, 7507 (2015).
- [12] S. Dai, J. Quan, G. Hu, C.-W. Qiu, T. H. Tao, X. Li, and A. Alù, *Nano Lett.* **19**, 1009 (2019).
- [13] N. C. Passler, X. Ni, G. Hu, J. Matson, G. Carini, M. Wolf, M. Schubert, A. Alù, J. Caldwell, T. Folland, and A. Paarmann, *Nature (London)* **602**, 595 (2022).
- [14] M. He, T. G. Folland, J. Duan, P. Alonso-González, S. De Liberato, A. Paarmann, and J. D. Caldwell, *ACS Photonics* **9**, 1078 (2022).
- [15] S. Dai, Q. Ma, T. Andersen, A. S. McLeod, Z. Fei, M. K. Liu, M. Wagner, K. Watanabe, T. Taniguchi, M. Thiemens, F. Keilmann, P. Jarillo-Herrero, M. M. Fogler, and D. N. Basov, *Nat. Commun.* **6**, 6963 (2015).
- [16] L. Ferrari, C. Wu, D. Lepage, X. Zhang, and Z. Liu, *Prog. Quantum Electron.* **40**, 1 (2015).
- [17] G. Hu, Q. Ou, G. Si, Y. Wu, J. Wu, Z. Dai, A. Krasnok, Y. Mazar, Q. Zhang, Q. Bao, C.-W. Qiu, and A. Alù, *Nature (London)* **582**, 209 (2020).
- [18] J. Duan, N. Capote-Robayna, J. Taboada-Gutiérrez, G. Álvarez-Pérez, I. Prieto, J. Martín-Sánchez, A. Y. Nikitin, and P. Alonso-González, *Nano Lett.* **20**, 5323 (2020).
- [19] Z. Zheng, F. Sun, W. Huang, J. Jiang, R. Zhan, Y. Ke, H. Chen, and S. Deng, *Nano Lett.* **20**, 5301 (2020).
- [20] M. Chen, X. Lin, T. H. Dinh, Z. Zheng, J. Shen, Q. Ma, H. Chen, P. Jarillo-Herrero, and S. Dai, *Nat. Mater.* **19**, 1307 (2020).
- [21] H. Herzig Sheinfux and F. H. L. Koppens, *Nano Lett.* **20**, 6935 (2020).
- [22] N. C. Passler and A. Paarmann, *J. Opt. Soc. Am. B* **34**, 2128 (2017).
- [23] N. C. Passler, M. Jeannin, and A. Paarmann, *Phys. Rev. B* **101**, 165425 (2020).
- [24] A. Otto, *Z. Phys. A: Hadrons Nucl.* **216**, 398 (1968).
- [25] N. C. Passler, I. Razzdolski, S. Gewinner, W. Schöllkopf, M. Wolf, and A. Paarmann, *ACS Photonics* **4**, 1048 (2017).
- [26] T. G. Folland, L. Nordin, D. Wasserman, and J. D. Caldwell, *J. Appl. Phys.* **125**, 191102 (2019).
- [27] E. Kretschmann, *Z. Phys.* **241**, 313 (1971).
- [28] B. Neuner, III, D. Korobkin, C. Fietz, D. Carole, G. Ferro, and G. Shvets, *Opt. Lett.* **34**, 2667 (2009).
- [29] N. C. Passler, C. R. Gubbin, T. G. Folland, I. Razzdolski, D. S. Katzer, D. F. Storm, M. Wolf, S. De Liberato, J. D. Caldwell, and A. Paarmann, *Nano Lett.* **18**, 4285 (2018).
- [30] D. C. Ratchford, C. J. Winta, I. Chatzakis, C. T. Ellis, N. C. Passler, J. Winterstein, P. Dev, I. Razzdolski, J. R. Matson, J. R. Nolen, J. G. Tischler, I. Vurgaftman, M. B. Katz, N. Nepal, M. T. Hardy, J. A. Hachtel, J. C. Idrobo, T. L. Reinecke, A. J. Giles, D. S. Katzer *et al.*, *ACS Nano* **13**, 6730 (2019).
- [31] A. Huber, N. Ocelic, D. Kazantsev, and R. Hillenbrand, *Appl. Phys. Lett.* **87**, 081103 (2005).
- [32] L. Novotny and S. J. Stranick, *Annu. Rev. Phys. Chem.* **57**, 303 (2006).
- [33] S. Dai, Z. Fei, Q. Ma, A. S. Rodin, M. Wagner, A. S. McLeod, M. K. Liu, W. Gannett, W. Regan, K. Watanabe, T. Taniguchi, M. Thiemens, G. Dominguez, A. H. C. Neto, A. Zettl, F. Keilmann, P. Jarillo-Herrero, M. M. Fogler, and D. N. Basov, *Science* **343**, 1125 (2014).
- [34] C. R. Gubbin, R. Berte, M. A. Meeker, A. J. Giles, C. T. Ellis, J. G. Tischler, V. D. Wheeler, S. A. Maier, J. D. Caldwell, and S. De Liberato, *Nat. Commun.* **10**, 1682 (2019).
- [35] A. Fali, S. T. White, T. G. Folland, M. He, N. A. Aghamiri, S. Liu, J. H. Edgar, J. D. Caldwell, R. F. Haglund, and Y. Abate, *Nano Lett.* **19**, 7725 (2019).
- [36] Gonzalo Álvarez-Pérez, T. G. Folland, I. Errea, J. Taboada-Gutiérrez, J. Duan, J. Martín-Sánchez, A. I. F. Tresguerres-Mata, J. R. Matson, A. Bylinkin, M. He, W. Ma, Q. Bao, J. I. Martín, J. D. Caldwell, A. Y. Nikitin, and P. Alonso-González, *Adv. Mater.* **32**, 1908176 (2020).
- [37] W. C. Chew, *Waves and Fields in Inhomogeneous Media* (Wiley-IEEE Press, New York, 1999).
- [38] N. C. Passler, G. Carini, and A. Paarmann, Layer-Resolved Resonance Intensity of Evanescent Polariton Modes in Anisotropic Multilayers (Matlab Files) (2022), doi:10.5281/zenodo.7034721.
- [39] Z. Sakotic, A. Krasnok, N. Cselyuska, N. Jankovic, and A. Alù, *Phys. Rev. Appl.* **13**, 064073 (2020).
- [40] S. Enoch, G. Tayeb, P. Sabouroux, N. Guérin, and P. Vincent, *Phys. Rev. Lett.* **89**, 213902 (2002).
- [41] J. Kim, A. Dutta, G. V. Naik, A. J. Giles, F. J. Bezares, C. T. Ellis, J. G. Tischler, A. M. Mahmoud, H. Caglayan, O. J.

- Glebocki, A. V. Kildishev, J. D. Caldwell, A. Boltasseva, and N. Engheta, *Optica* **3**, 339 (2016).
- [42] C. Argyropoulos, P.-Y. Chen, G. D'Aguanno, N. Engheta, and A. Alù, *Phys. Rev. B* **85**, 045129 (2012).
- [43] H. Suchowski, K. O'Brien, Z. J. Wong, A. Salandrino, X. Yin, and X. Zhang, *Science* **342**, 1223 (2013).
- [44] M. G. Silveirinha and N. Engheta, *Phys. Rev. B* **76**, 245109 (2007).
- [45] B. Edwards, A. Alù, M. G. Silveirinha, and N. Engheta, *J. Appl. Phys.* **105**, 044905 (2009).
- [46] S. Vasant, J.-P. Hugonin, F. Marquier, and J.-J. Greffet, *Opt. Express* **20**, 23971 (2012).
- [47] L. Nordin, O. Dominguez, C. M. Roberts, W. Streyer, K. Feng, Z. Fang, V. A. Podolskiy, A. J. Hoffman, and D. Wasserman, *Appl. Phys. Lett.* **111**, 091105 (2017).
- [48] S. Campione, I. Brener, and F. Marquier, *Phys. Rev. B* **91**, 121408(R) (2015).
- [49] J. J. Burke, G. I. Stegeman, and T. Tamir, *Phys. Rev. B* **33**, 5186 (1986).